JOURNAL OF PROPULSION AND POWER
Vol. 21, No. 3, May–June 2005

Magnetohydrodynamic Instabilities in a Simple Gasdynamic Mirror Propulsion System

William J. Emrich Jr.*
NASA Marshall Space Flight Center, Huntsville, Alabama 35812
and
Clark W. Hawk†
University of Alabama at Huntsville, Huntsville, Alabama 35899

The gasdynamic mirror has been proposed as a concept that could form the basis of a highly efficient fusion rocket engine. Gasdynamic mirrors differ from most other mirror-type plasma confinement schemes in that they have much larger aspect ratios and operate at somewhat higher plasma densities. To evaluate whether a gasdynamic mirror could indeed confine plasmas in a stable manner for long periods of time, a small-scale experimental gasdynamic mirror was built and tested. The objective of this experiment was to determine ranges of mirror ratios and plasma densities over which a gasdynamic mirror could maintain stable plasmas. Theoretical analyses indicated that plasma magnetohydrodynamic (MHD) instabilities were likely to occur during subsonic to supersonic flow transitions in the throat region of the gasdynamic mirror. The experimental evidence, based on data derived from langmuir probe measurements, seems to confirm this analysis. The assumption that a gasdynamic mirror using a simple mirror geometry could be used as a propulsion system, therefore, appears questionable. Modifications to the simple mirror concept are presented that could mitigate these MHD instabilities.

Nomenclature

A	=	cross-sectional area
A_{pc}	=	cross-sectional area of plasma in main chamber
A_{pm}	=	cross-sectional area of plasma at mirror throat
A^*	=	plasma cross-sectional area at which sonic flow occurs
B	=	local magnetic field strength
B_{pc}	=	magnetic field strength in plasma at center of main chamber
B_{pm}	=	magnetic field strength in plasma at mirror throat
c	=	speed of sound
I_{sp}	=	specific impulse
j_{max}	=	number of points comprising measured plasma density or temperature profile
K	=	specific heat ratio
k_n	=	plasma wave propagation vector normal to magnetic field
l	=	position
M_c	=	chamber Mach number
M_t	=	throat Mach number
m	=	atomic weight of plasma ions
$\dot{m}$	=	mass flow rate
n	=	plasma density
P	=	local total plasma pressure
$P_\parallel$	=	component of pressure parallel to magnetic field
$P_\perp$	=	component of pressure perpendicular to magnetic field
P^*	=	pressure in nozzle throat at Mach 1
R	=	vacuum mirror ratio
R_c	=	radius of curvature of magnetic field
R_e	=	effective mirror ratio accounting for finite plasma pressure
R_u	=	universal gas constant
r	=	radius
T	=	plasma ion temperature
t_{95}	=	t distribution 95% confidence limit
U	=	uncertainty value
V	=	particle velocity
$V_\parallel$	=	particle velocity parallel to magnetic field
$V_\perp$	=	particle velocity perpendicular to magnetic field
$\langle v \rangle$	=	average particle velocity
α	=	mirror loss cone angle
β	=	ratio of plasma pressure to magnetic pressure
γ	=	plasma magnetohydrodynamic instability growth rate
σ	=	standard deviation of measured plasma density
Φ_{pc}	=	plasma flux in central chamber
Φ_{pm}	=	plasma flux at mirror throat
Ψ	=	ratio of plasma cross-sectional area at mirror throat to mirror throat cross-sectional area required for sonic flow

Introduction

THE large-scale human exploration of the solar system will require the transportation of massive amounts of equipment and supplies over vast distances in space in relatively short periods of time. These requirements place a heavy burden on the rocket engines carrying out these missions. Studies have shown that chemical propulsion systems can perform piloted missions only to the closest planets and even those only with great difficulty.[1] Piloted flights beyond Mars do not appear to be possible with chemical systems, regardless of the vehicle configuration. The inadequacy of traditional rocket engines is due to the energy density of chemical propellants being limited. This limitation puts restrictions on the maximum rocket engine efficiency and, consequently, limits the scope of the missions that can be executed. One type of propulsion system that appears to have the potential to provide the performance levels required for fast interplanetary travel is based on the use of fusion energy. Recent studies[2,3] indicate that space vehicles employing fusion propulsion systems could be constructed with specific powers of 10 or greater. At these performance levels, a one-way mission to Mars could be accomplished in 40 days, and a one-way mission to Pluto could be accomplished in about two years. For comparison, a NASA study,[4] concluded that a Mars mission using only chemical propulsion would require a 490-day round trip flight time (156 days outbound) and would require aerobraking at Mars to reduce fuel requirements to a manageable level.

One type of fusion reactor that has been proposed as the basis for a spacecraft propulsion system is the gasdynamic mirror. This type of device has been theorized to have fairly high specific powers and

Received 12 December 2003; revision received 4 December 2004; accepted for publication 4 December 2004.

*Engineer, Propulsion Research Center. Member AIAA.
†Professor, Propulsion Research Center. Fellow AIAA.

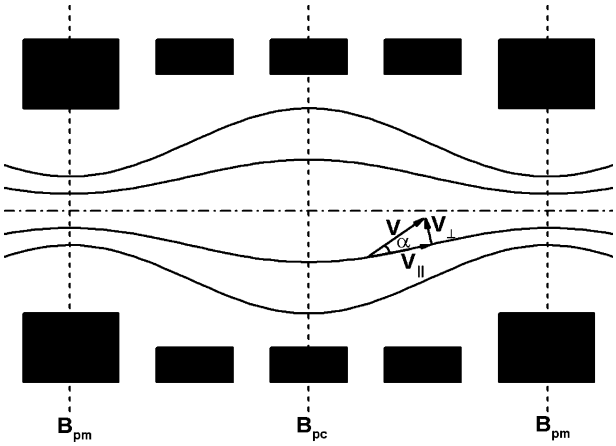

Fig. 1 Particle motion in a mirror.

specific impulses as high as 100,000 s (Ref. 5). Magnetic mirror reactors are well suited for spacecraft propulsion system applications because their open-ended linear geometry allows a natural path for the fusioning plasma exhaust. Mirror-type fusion devices use a magnetic field line configuration called a magnetic well to confine the charged plasma particles. Plasma confinement has improved over the years with the newer mirror systems, although this improvement has generally come at the cost of increased complexity in the magnetic coil configurations at the mirrors. Mirror machines consist mainly of large multisegment solenoids surrounding a vacuum chamber containing the plasma. A schematic diagram of a magnetic mirror machine illustrating a typical magnetic field configuration is shown in Fig. 1. The bulk of the fusion plasma is confined by magnetic fields generated within the central solenoid by a series of toroidal-shaped magnets. Stronger toroidal end magnets called mirror magnets prevent the plasma from escaping too quickly out of the ends. The ratio of the maximum magnetic field strength in the mirrors divided by the minimum magnetic field strength in the central solenoid is called the mirror ratio R, and it is generally found that increasing the mirror ratio improves plasma confinement. Confinement is achieved in mirror machines because of constraints on particle motion imposed by the conservation of magnetic moment and the conservation of energy. Better confinement is especially desirable from a propulsion system standpoint because it translates directly into shorter system lengths and reduced mass. Previous analyses suggest that for gasdynamic mirror systems, the length necessary to achieve self-sustained fusion is inversely proportional to the mirror ratio.

Raising the mirror ratio to high values to increase plasma confinement is not always effective because high mirror ratios can also induce the occurrence of certain rather severe plasma instabilities in the device called magnetohydrodynamic (MHD) instabilities. These instabilities are a result of convex curvature in the magnetic field lines with respect to the machine centerline. In simple mirror machines, convex magnetic field line curvature occurs naturally in the main chamber region of the device, especially near the mirror magnets, and is accentuated by increases in the mirror ratio. The curvature of the magnetic field causes charge separation to occur between the electrons and the ions in the plasma. Electric fields induced by this charge separation cause uncontrollable ion drifts across the magnetic field lines that result in the appearance of plasma "flutes" that extend radially outward from the centerline of the plasma column (Fig. 2). These flutes lead to a rapid loss of confinement as the plasma impacts the containment walls. This instability is also known as the interchange instability because a geometrical view of the process reveals that there is an interchange between the magnetic flux originally outside the plasma boundary and the plasma inside the plasma boundary. The degree to which the plasma may be made to remain stable is thought to be determined primarily by the relative density of plasma in regions of the device having convex "bad" magnetic curvature compared to the density of plasma in

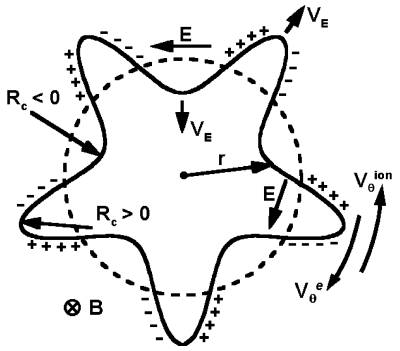

Fig. 2 MHD flute instability.

regions of the device having concave "good" magnetic curvature. Because subsonic to supersonic flow transitions cause the plasma density distribution to change drastically in regions of pronounced magnetic field curvature, a knowledge of flow transition effects with regard to plasma stability is crucial if magnetic mirror devices are to form the basis of spacecraft propulsion systems.

The plasma stability achieved with the gasdynamic trap at Novosibirsk, Russia[6] suggests that rocket engines based on similar designs should be feasible. Gasdynamic mirror devices have the advantage of being simple in construction and, because they operate with plasma densities that are relatively high, they should provide good thrust to weight ratios. These advantages, however, are contingent on the gasdynamic mirror operating in a stable manner under conditions in which self-sustained fusion occurs, for example, plasma densities $>10^{15}$ cm^{-3} and plasma temperatures $>10^{8}$ K. To confirm the expected operational characteristics of a magnetic mirror-based fusion propulsion system, a study was undertaken to examine theoretically and experimentally how plasma density variations between the convex and concave regions of magnetic field line curvature in a mirror device affect plasma stability.

MHD Instabilities

The stability of plasmas in magnetic fields was first studied extensively by Rosenbluth and Longmire.[7] Their analysis established a fairly simple criterion whereby the stability of plasmas could be evaluated where the stability factor is

$$\int \frac{P_{\parallel}(l) + P_{\perp}(l)}{r R_c(l) B^2(l)}\, \mathrm{d}l \overset{\text{for stability}}{<} 0 \qquad (1)$$

The geometrical factors in Eq. (1) are illustrated in Fig. 2.

The gasdynamic mirror attempts to establish a stable plasma configuration by creating a long straight central region with little curvature in the magnetic field lines ($R_c = 0$), a short transition of bad curvature, and a throat region of good curvature with significant plasma pressure. A previous analysis[8] of a gasdynamic mirror in which the velocity of the exit flow was limited to a low supersonic value implied that stable operation was possible. If the plasma exhaust jet is allowed to expand freely, as would be the case for a propulsion system, other results are possible. Applying Eq. (1) to the gasdynamic mirror (GDM) using flow parameters and axial magnetic field profiles typical of the current experiment, along with standard compressible flow equations, it is possible to draw a number of additional interesting conclusions regarding MHD stability in the GDM.

Figure 3 illustrates how the stability factor varies as Eq. (1) is integrated along the GDM axis. Figure 3 reveals how quite different stability results can be manifest from two almost identical supersonic main chamber plasma flow profiles.

In one case, the plasma flow is adjusted so that it remains slightly supersonic in the mirror throat, resulting in a flow that remains supersonic in the diverging section of the magnetic mirror. In the other case, the flow is increased slightly so that a sonic condition occurs in the mirror throat resulting in a flow transition to subsonic in the diverging section of the magnetic mirror. It will be shown

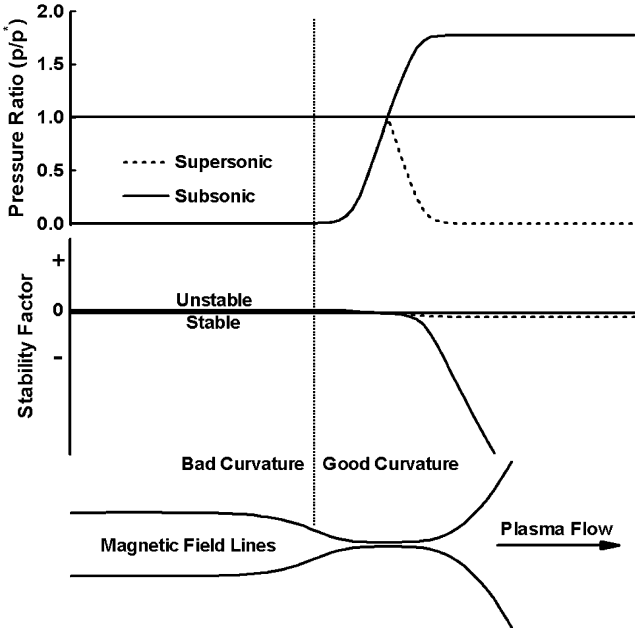

Fig. 3 MHD instability with supersonic chamber flow.

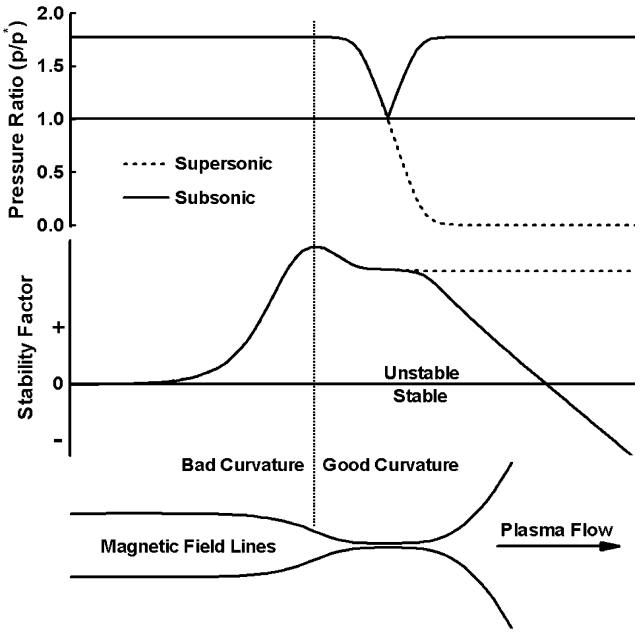

Fig. 4 MHD instability with subsonic chamber flow.

that the transition to subsonic flow in the mirror throat results in a strong stabilizing effect on the plasma due to the high plasma density in this region of good magnetic curvature. Unfortunately, subsonic exhaust flows are not very desirable from a rocket engine efficiency point of view. This poor efficiency is due to I_{sp} being proportional to the propellant exhaust velocity. If the plasma remains supersonic throughout the throat region and beyond, the plasma should still remain stable, though only marginally. This stability is the result of a fairly significant pressure spike that occurs primarily in the region of good magnetic curvature near the throat of the GDM.

Figure 4 illustrates how the stability factor varies as Eq. (1) is integrated along the GDM axis using two, almost identical, subsonic main chamber plasma flow profiles. In one case, the plasma flow is adjusted so that it remains slightly subsonic in the mirror throat, resulting in a flow that remains subsonic in the diverging section of the magnetic mirror. In the other case, the flow is increased slightly so that a sonic condition occurs in the mirror throat, resulting in a flow transition to supersonic in the diverging section of the magnetic mirror. It will be shown that a transition to supersonic flow in the mirror throat results in the plasma being highly unstable. The instability is caused by the plasma pressure decreasing rapidly throughout the diverging region of the magnetic mirror. In essence, the stabilizing effect of plasma in the region of good magnetic curvature near the mirror throat is overwhelmed by the destabilizing effect of the much higher density plasma in the converging section of the magnetic mirror where the magnetic curvature is bad. This situation is unfortunate because the normal flow distribution in rocket nozzles is generally similar to that just described. To compensate for this situation, it may be possible to externally inject high-density, low-temperature plasma into the diverging section of the magnetic mirror nozzle to raise the overall plasma density in this region of good magnetic curvature to the point where plasma stability may be restored. Whether this can be effectively done remains to be seen, however, and at this point such a remedy remains highly speculative. Nevertheless, if such a procedure were effective, it would be highly beneficial to the engine system in that it would increase the thrust level and reduce the specific impulse. Because for many planetary missions, the specific impulse of the GDM is significantly higher than necessary, external plasma injection, if effective, would solve two problems at once by increasing plasma stability and providing a more optimum thrust and specific impulse combination.

If the flow is prevented from going supersonic in the throat, but instead remains subsonic throughout the flow regime, stability may be regained if the plasma does not detach from the magnetic field lines until it is relatively far downstream of the throat. This flow configuration would not require external plasma injection, but it also may not constitute a particularly desirable state. Because much of the exhaust will not be parallel to the direction of flight, the engine will experience a considerable loss of propulsive efficiency.

Experimental Setup

To verify experimentally the theoretical predictions as outlined earlier, a small GDM was built at the NASA Marshall Space Flight Center. Although the machine currently operates at temperatures far too low to initiate any fusion reactions, the geometric configuration is such that it should be able to answer many of the fundamental questions on plasma stability in the GDM. Because it was anticipated that a wide variety of plasma conditions would be eventually studied using the GDM device, much effort was expended in designing it to be as flexible and expandable as possible from the beginning. Table 1 lists the major physical characteristics of the GDM in its current configuration.

The GDM experiment was constructed in a modular fashion containing at a minimum two mirror segments and a main segment. This minimum configuration was the setup used in the present set of experiments. A provision has been made to allow for the addition of more main segments at a future date, thus enabling the experiment to grow easily without the need for an extensive redesign. Each segment has been designed to operate independently of the others to the

Table 1 GDM experiment physical characteristics

Description	Value
Length (main chamber)	2.0 m
Length (mirror chambers plus one main chamber)	2.5 m
Main chamber diameter	20 cm
Mirror chamber diameter	6 cm
Number of magnets per main chamber	17
Number of magnets per mirror chamber	12
Magnet current	up to 3000 A
Main chamber vacuum magnetic field	up to 0.35 T (centerline)
Mirror chamber vacuum magnetic field	up to 2.05 T (centerline)
Vacuum chamber length	1.5 m
Vacuum chamber diameter	1.2 m
Vacuum pumping speed	800 l/s
Microwave injector power	1000 W
Microwave injector frequency	2.45 GHz

greatest extent practical. The water-cooled copper magnets in each segment are controlled by their own power supplies and are fed by their own header systems. By the independent control of the power to each set of magnets, great flexibility is obtained with regard to being able to shape the magnetic fields within the device. Each of the mirror segments also has a small subsegment near the interface to the main chamber segment. This subsegment was designed to allow flexibility for future modifications to the mirror segments to enable the incorporation of such things as confinement enhancing devices, additional diagnostics, etc.

A closed-loop cooling system flows cold water along a distribution system that runs along the entire length of the experiment. This water distribution system has a series of valves and quick disconnects to enable the segments to be easily broken apart when the experiment is reconfigured. The cooling system consists of a 300-gal reservoir for the cooling water, a water-to-water heat exchanger, and a pump. Cold service water flows through the primary side of the heat exchanger, and the water pump forces the cooling water from the reservoir through the experiment and finally to the secondary side of the heat exchanger.

The two mirror segments, which form the ends of the GDM, are used to restrict the plasma loss from the system and have many common features. Each mirror segment has a vacuum pumping system that consists of a roughing pump and a turbopump, and each has two power supplies. There are 12 magnets in each mirror, one-half of which are connected to each power supply. Limited field shaping is, thus, possible in the mirrors. Water boost pumps are used to circulate coolant through the magnets because the heating rates will be considerably larger in the mirror magnets as compared to the central segment magnets.

Although the mirror segments serve the same primary purpose, they have quite different secondary purposes. One mirror segment contains a large vacuum chamber that serves several purposes. First, the chamber can serve as a vacuum reservoir for the exhaust during high-flow plasma tests. For these tests, the pumping system will be unable to maintain the desired downstream vacuum, and the vacuum chamber will allow these tests to be conducted, albeit for limited durations. Second, the vacuum chamber could also serve as a means by which the plasma exhaust may be studied after the plasma leaves the GDM because many questions still exist as to how the plasma may be made to detach efficiently from the magnetic field lines after it leaves the device.

The other mirror segment contains the plasma injector and control circuitry. Currently, the plasma is generated and heated by a microwave device that is described hereafter. The segment has been constructed to allow various types of plasma injectors to be used in the system. These injectors may be mounted either before or after the mirror.

The central segment contains the bulk of the plasma in the GDM experiment. This segment is basically a 20-cm-diam vacuum tube containing various diagnostic ports and surrounded by 17 magnets. These magnets can produce central fields of up to one-third of a tesla when operated at full current by the single power supply associated with this segment. The main chamber is attached to the mirror segments by short bellows connectors that permit a tight vacuum to be maintained along the length of the GDM. As was stated earlier, the design of the experiment allows multiple central segments to be easily incorporated into the device.

Control and monitoring functions for the GDM experiment are accomplished through the use of a computer program that checks a series of transducers that measure temperatures, flowrates, etc. in various parts of the device and also controls the operation of the various pumps and power supplies.

Figure 5 shows the magnetic field lines near the GDM injector segment. The magnetic field in the GDM is generated by a series of water-cooled toroidal-shaped magnets spaced periodically along the lengths of the main and mirror segments. The spacing between the magnets in the main chamber is large enough to allow diagnostic probes to be inserted between them, but not so large as to create significant ripples in the magnetic field within the main plasma chamber. Even near the edge of the chamber where field variations

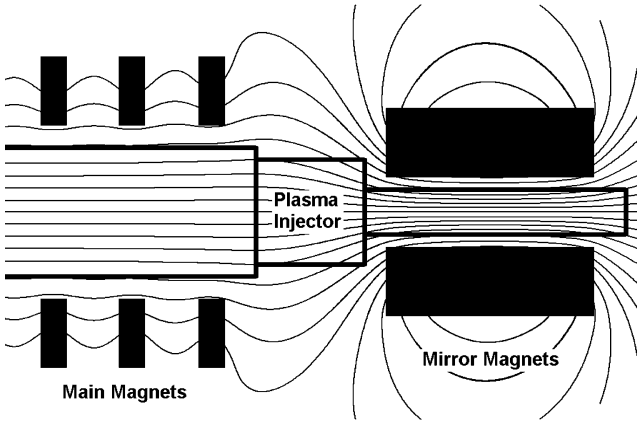

Fig. 5 Magnetic field lines near GDM injector segment.

are greatest, the ripple is only from 3 to 4%. A short distance away from the mirrors, the magnetic field becomes quite flat. This flat profile is quite important in minimizing plasma MHD instabilities, as will be discussed later.

Plasma heating in the GDM is accomplished through the use of a small plasma injector system located between the main chamber magnets and the mirror magnets. The purpose of the plasma injector is to introduce a gas (typically argon) into the GDM and to heat it until it becomes a plasma. The injector operates by using a microwave antenna operating at 2.45 GHz to induce electron cyclotron resonance heating of the gas. The heating occurs when the magnetic field strength is such that the electrons resonate at the microwave injector frequency. This requirement imposes an operational constraint on the plasma injector system in that the magnetic field within the device must at some point correspond to the microwave injector frequency. Once the electrons have been heated by the microwaves, they will stream out of the injector and into the main plasma chamber in response to an imposed magnetic field gradient. In doing so, they create an electric field that drags the ions along through a process called ambipolar diffusion. It is this process of ambipolar diffusion that increases the directed kinetic energy of the ions through energy transfer from the electrons.

Experimental Results

The experimental program for the GDM consisted of a series of plasma density and temperature measurements designed to define the stability limits of the device in terms of the vacuum chamber mirror ratio and the argon flow rate. To this end, the mirror ratio at the vacuum chamber end of the GDM was varied from 3 to 15 using argon flow rates fixed at either 2.5 or 6.0 standard cm^3/min (SCCM). The mirror ratio was varied solely by adjusting the magnetic field strength of the vacuum chamber segment mirror magnets. The main chamber magnets and the mirror magnets at the plasma injector end of the GDM were held fixed to maintain a constant injector segment mirror ratio of nine. Holding the injector segment mirror ratio constant was necessary because the plasma ion energy distribution varies as a function of the injector mirror ratio and a varying ion energy distribution could cause inconsistent results.

From langmuir probe measurements, average values for plasma density and electron temperature were calculated for the argon plasma column. These measurements were taken near the center of the main vacuum chamber. An analysis of these parameters yields information that can indicate the presence of plasma instabilities. Instabilities cause perturbations to occur in the plasma (flutes for MHD instabilities and turbulence for microinstabilities) that result in the plasma rapidly diffusing across the confining magnetic field lines. Because the confining capability of mirror machines largely depends on the relative diameter of the throat area through which the plasma can escape, any perturbation that enhances cross-field diffusion effectively enlarges the mirror throat area, resulting in an increase in plasma loss rate. Because increases in the plasma loss rate limit the density that can be sustained in the device, instabilities

Table 2 Typical experimental GDM plasma parameters

Parameter	Value
Plasma density, ion/cm^3	10^{13}
Electron temperature, eV	2
Beta	0.003
Plasma diameter in main chamber, cm	4
Plasma confinement time, ms	10
n τ, ion · s/cm^3	10^{11}
Plasma ion collision mean free path, cm	0.1

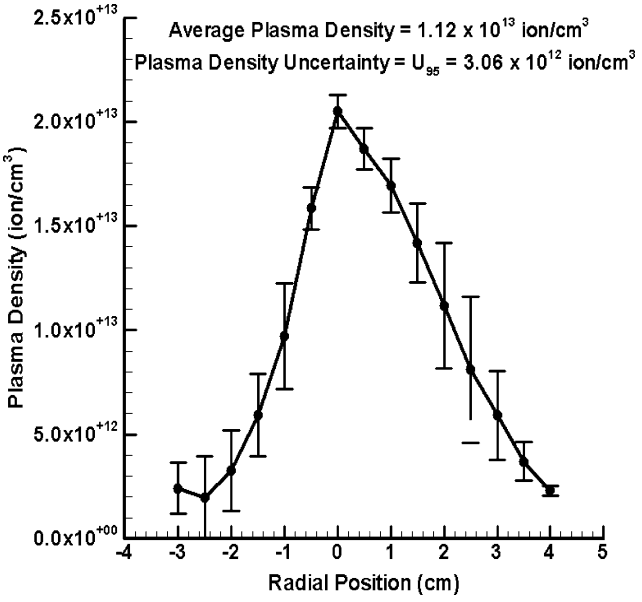

Fig. 6 Averaged langmuir probe data.

will be detectable by drops in the plasma density and reduced confinement times. Table 2 lists typical values observed during the experiments for several plasma parameters.

Uncertainty Analysis

Several scans were made at each mirror ratio and argon flow rate, and the results were combined to yield composite plasma density and electron temperature profiles. Because the positions of the density and temperature measurements varied from scan to scan, a linear interpolation was performed between adjacent measurement points within a profile to yield data values that could be placed on an evenly spaced grid. The data values thus placed on the grid from the various individual profiles were then averaged, and standard deviations were computed to yield the composite density or temperature profile. The average plasma density or electron temperature for each individual profile was also calculated to permit the determination of the composite average values for those parameters, along with their standard deviations for that particular combination of mirror ratio and argon flow rate. Figure 6 shows an example of an averaged plasma density profile.

Data Averaging

To perform the required plasma stability calculations, it was necessary to obtain profile averages of the plasma density and temperature. The average value for plasma density n was calculated by taking the composite plasma density profile and area weighting the pointwise plasma densities centered around the point of maximum plasma density. The calculation proceeded using the following equation:

$$n = \left(\sum_{j=1}^{j_{\max}} A_j n_j\right) \Big/ \left(\sum_{j=1}^{j_{\max}} A_j\right) = \left(\sum_{j=1}^{j_{\max}} A_j n_j\right) \Big/ A \qquad (2)$$

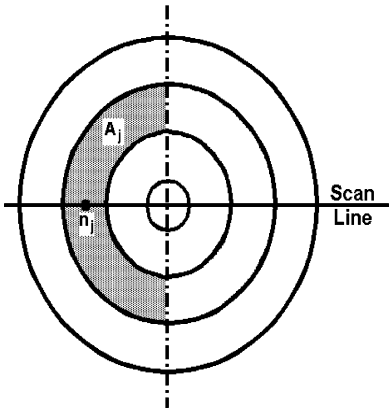

Fig. 7 Plasma areas used in data averaging.

where n_j is the plasma density corresponding to plasma cross-sectional area A_j (Fig. 7). The plasma temperature T was averaged in a similar manner, except that it was weighted with both area and plasma density to obtain an energy-averaged temperature. This averaging proceeded using a weighting equation of the form

$$T = \left(\sum_{j=1}^{j_{\max}} A_j n_j T_j\right) \Big/ \left(\sum_{j=1}^{j_{\max}} A_j n_j\right) \qquad (3)$$

The uncertainties U in the average plasma density and temperature were calculated by using the general uncertainty equation,[9] which, when applied to the present situation, yields for the uncertainty in plasma density

$$U_n^2 = \sum_{j=1}^{j_{\max}} \left[\left(\frac{\partial n}{\partial A_j}\right)^2 U_{A_j}^2 + \left(\frac{\partial n}{\partial n_j}\right)^2 U_{n_j}^2\right] = \sum_{j=1}^{j_{\max}} \left(\frac{A_j}{A}\right)^2 U_{n_j}^2 \qquad (4)$$

For the uncertainty in the electron temperature, the uncertainty equation is given by

$$U_T^2 = \sum_{j=1}^{j_{\max}} \left[\left(\frac{\partial T}{\partial A_j}\right)^2 U_{A_j}^2 + \left(\frac{\partial T}{\partial n_j}\right)^2 U_{n_j}^2 + \left(\frac{\partial T}{\partial T_j}\right)^2 U_{T_j}^2\right]$$

$$= \sum_{j=1}^{j_{\max}} \left(\left\{\left[A_j T_j \left(\sum_{k=1}^{j_{\max}} A_k n_k\right) - A_j^2 n_j T_j\right] \Big/ \left(\sum_{k=1}^{j_{\max}} A_k n_k\right)^2\right\}^2 U_{n_j}^2 + \left[A_j N_j \Big/ \left(\sum_{k=1}^{j_{\max}} A_k n_k\right)\right]^2 U_{T_j}^2\right) \qquad (5)$$

The uncertainties in plasma density and electron temperature in Eqs. (4) and (5) represent the 95% confidence limits on the respective measurements and were calculated from the standard deviations as follows

$$U_n = \sigma_n t_{95} \Big/ \sqrt{j_{\max}}, \qquad U_T = \sigma_T t_{95} \Big/ \sqrt{j_{\max}}, \qquad U_A \approx 0 \qquad (6)$$

where U_A is small compared to U_n and U_T.

MHD Stability Results

Earlier, it was theorized that MHD plasma instabilities should occur during subsonic to supersonic flow transitions in the mirror throat region of the GDM. These instabilities result in a loss of plasma confinement and are indicated by decreases in measured plasma density. As the mirror ratio is increased, the throat area through which the plasma flows decreases. At a given flow rate a mirror ratio is eventually reached where the flow goes sonic at the throat, resulting in supersonic flow downstream. This mirror ratio is the maximum mirror ratio under which stable operation is possible and yields the maximum plasma density possible for that configuration.

To calculate the mirror throat Mach number, the flow velocity $\langle v \rangle$ in the main chamber is first determined from the continuity equation

$$\langle v \rangle = \dot{m}/nA_{\rm pc} \tag{7}$$

In Eq. (7), the flow rate $\dot{m}$ is that which was set during the experiment, and the plasma density n and plasma main chamber cross-sectional area $A_{\rm pc}$ are derived from the langmuir probe measurements. The plasma cross-sectional area was calculated on the basis of the diameter of the plasma column within which the data were deemed to be valid. Under the test conditions used in this study, the plasma column diameter was about 4 cm, with data outside this range showing no clear probe characteristic. The plasma sonic velocity was determined from the equation

$$c = \sqrt{(KR_uT)/m} \tag{8}$$

The temperature T in Eq. (8) was obtained from langmuir probe measurements and is technically the electron temperature. It is assumed for this calculation, however, that the collisionality between the electrons and ions is such that thermodynamic equilibrium has been reached and that the temperatures for the two species can be taken to be the same. This assumption should be quite valid because with an ion mean free path of about 0.1 cm, the ions will suffer hundreds of collisions with electrons before they reach the langmuir probe, which is located near the center of the GDM. The Mach number in the main chamber can be calculated by

$$M_c = \langle v \rangle / c \tag{9}$$

The chamber Mach number calculated in Eq. (9) is then used in the isentropic compressible flow equation for simple area change[10] to determine the plasma cross-sectional area ratio required to achieve sonic flow at the mirror throat

$$\frac{A_{\rm pc}}{A^*} = \frac{1}{M_c}\sqrt{\left[\frac{2}{K+1}\left(1+\frac{K-1}{2}M_c^2\right)\right]^{(k+1)/(k-1)}} \tag{10}$$

The actual plasma cross-sectional area ratio at the mirror throat is estimated by noting that, because of the conservation of magnetic flux lines,

$$\Phi_{\rm pc} = \Phi_{\rm pm} \Rightarrow B_{\rm pc}A_{\rm pc} = B_{\rm pm}A_{\rm pm} \Rightarrow A_{\rm pc}/A_{\rm pm} = B_{\rm pm}/B_{\rm pc} = R \tag{11}$$

The results obtained from Eqs. (10) and (11) may be combined to obtain a relation that yields the ratio of the actual area of the plasma at the mirror throat to the area of the throat that would be required to achieve sonic flow

$$\Psi = \frac{A_{\rm pm}}{A^*} = \frac{1}{R}\frac{A_{\rm pc}}{A^*}$$

$$= \frac{1}{RM_c}\sqrt{\left[\frac{2}{K+1}\left(1+\frac{K-1}{2}M_c^2\right)\right]^{(k+1)/(k-1)}} \tag{12}$$

The uncertainty in the measured values for Ψ may be calculated by first determining the uncertainty in the measured Mach number by using Eqs. (7–9) in the general uncertainty equation. The resulting relation is then given by

$$U_M^2 = \left(\frac{\partial M}{\partial n}\right)^2 U_n^2 + \left(\frac{\partial M}{\partial T}\right)^2 U_T^2 = \frac{\dot{m}^2}{KR_uA^2n^2T}\left(\frac{U_n^2}{n^2}+\frac{U_T^2}{4T^2}\right) \tag{13}$$

The uncertainty in Ψ can now be determined by again applying the general uncertainty equation using the relations described by Eqs. (12) and (13):

$$U_\Psi^2 = \left(\frac{\partial \Psi}{\partial M}\right)^2 U_M^2$$

$$= \frac{2\sqrt{2}(M^2-1)\sqrt{\{1+[(K-1)/2]M^2\}^{(K+1)/(K-1)}}}{RM^2[2+(K-1)M^2]\sqrt{K+1}}U_M^2 \tag{14}$$

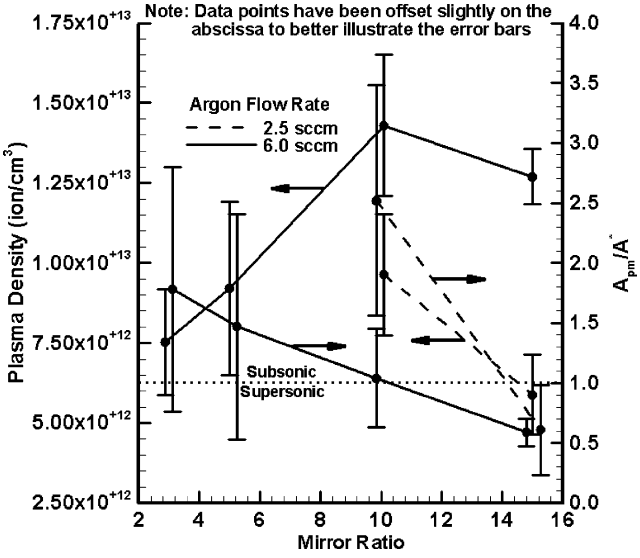

Fig. 8 Measured mirror ratio effects on plasma density.

The uncertainty term associated with the mirror ratio has been neglected in Eq. (14) because its uncertainty is small compared to the uncertainties in plasma density and electron temperature.

Note that the mirror ratio used in Eq. (12) is the effective mirror ratio that the plasma sees and not the vacuum mirror ratio, which is only a ratio of the mirror to central magnetic field strengths. The effective mirror ratio takes into account the effects of plasma pressure and is related to the vacuum mirror ratio by the following relation[11]

$$R_e = R\Big/\sqrt{1-\beta} \tag{15}$$

If the plasma pressure is considerably less than the magnetic pressure ($\beta \ll 1$), the two values differ by only a small amount, and the error introduced by using only the vacuum mirror ratio in the calculations is small. Because the plasma should remain stable if M_t is less than one (all subsonic flow), it follows that values of $A_{\rm pm}/A^* > 1$ must be maintained if stable plasma conditions are to be achieved. To confirm this conjecture, a set of measurements covering mirror ratios between 3 and 15 was performed at an argon flow rate of 6.0 SCCM. From Fig. 8, which correlates plasma density with mirror ratio and $A_{\rm pm}/A^*$, it is apparent that a fairly significant decrease in plasma density seems to occur between mirror ratios of 10 and 15. Because the plasma flow transitions to supersonic in this mirror ratio regime also, it was strongly suspected that MHD instabilities were present. This suspicion was bolstered by the growth rate of MHD instabilities under normal experimental conditions being found to be much faster than the loss rate of plasma from the device. The growth rate γ of the MHD instabilities was determined using a procedure described in Ref. 12 and is based on an analysis of the plasma drift acceleration in curved magnetic fields. This plasma acceleration yields a growth rate of the form

$$\gamma = \sqrt{\left[\left(v_\perp^2/2 + v_\parallel^2\right)/R_c\right]k_n} \tag{16}$$

Using parameter values characteristic of the GDM experiments at the point of maximum bad curvature yields results that indicate that MHD instabilities will begin to manifest themselves in about 5×10^{-4} s. Because the confinement time of plasma particles in the GDM was measured to be about 0.01 s, it was concluded that MHD disruptions were the likely cause of the observed plasma density decreases. Other experimental runs to confirm the presence of MHD instabilities were performed under different conditions using an argon flow rate of 2.5 SCCM. These runs, which concentrated only on the subsonic to supersonic flow transition region, showed a behavior similar to that observed at the higher flow rate. Similar drops in plasma density at certain critical values of R have also been observed in Russian experiments with the gasdynamic trap at Novosibirsk,[13] although it was impossible to confirm from the data

presented that the plasma density drops occurred at the point of subsonic to supersonic transition.

Conclusions

The results of the GD Mirror propulsion experiment indicate that MHD instabilities are likely to occur as a result of subsonic to supersonic flow transitions in the plasma exhaust stream. These instabilities result in a loss of plasma confinement and would almost certainly prevent the initiation of fusion reactions. As a result, the assumption that a GDM using a simple mirror geometry could be used as a propulsion system appears to be questionable. To overcome the stability problems in a GDM some sort of modification to the simple mirror concept will be required. Because the stability problem appears to be associated with the low plasma density associated with the transition to supersonic flow, it may be possible to stabilize the plasma through cold plasma injection into the hot plasma exhaust stream downstream of the mirror throat. This plasma injection would raise the plasma density in the regions of good magnetic curvature (the magnetic mirror nozzle throat and diverging section) to the point that the stability criterion as presented by Eq. (1) would be satisfied. The plasma injection would also help to reduce the inherently high specific impulse of the GDM and at the same time increase its thrust to weight level to values more appropriate for solar system travel. Whether it is possible to achieve these results from a practical standpoint remains to be seen, however, and further work will be required.

Acknowledgments

This work was financially supported by NASA. The authors are grateful to Terry Kammash of the University of Michigan for the many useful discussions that occurred during the course of this work. We wish to also thank the many others at NASA the Marshall Space Flight Center who participated in the construction of the gasdynamic mirror experiment and who contributed materially to the success of this work.

References

[1]Schulze, N., "Fusion Energy for Space Missions in the 21st Century," NASA TM 4298, Aug. 1991, Chap. 2.

[2]Kammash, T., and Emrich, W., "Interplanetary Missions with the GDM Propulsion System," *Proceedings of the 15th Symposium on Space Nuclear Power and Propulsion*, edited by M. El-Genk, AIP Conf. Proc. No. 420, Vol. 3, American Inst. of Physics, New York, 1998, pp. 1145–1150.

[3]Emrich, W., and Kammash, T., "Performance Optimization of the Gasdynamic Mirror Propulsion System," *Proceedings of the 17th Symposium on Space Nuclear Power and Propulsion*, edited by M. El-Genk, AIP Conf. Proc. No. 504, Vol. 1, American Inst. of Physics, New York, 2000, pp. 1420–1424.

[4]NASA Marshall Space Flight Center SEI Technical Study Team, "Space Exploration Initiative—Mars Transportation System Nuclear Thermal Rocket Propulsion Application (Addendum)," Internal Marshall Space Flight Center Rept., Huntsville, AL, June 1992.

[5]Kammash, T., and Lee, M. J., "Gasdynamic Fusion Propulsion System for Space Exploration," *Journal of Propulsion and Power*, Vol. 11, No. 3, 1995, p. 544.

[6]Bagryanskij, P. A., Ivanov, A. A., Klesov, V. V., Koz'minykh, Y. L., Kotel'nikov, I. A., Krasnikov, Y. I., Podyminogin, A. A., Rogozin, A. I., Rosylyakov, G. V., and Ryutov, D. D., "First Experiments on the Gasdynamic Trap," *Nuclear Fusion Supplement*, Vol. 3, 1987, pp. 467–476.

[7]Rosenbluth, M. N., and Longmire, C. L., *Annals of Physics*, Vol. 1, No. 2, 1957, pp. 120–140.

[8]Nagornyj, V. P., Ryutov, D. D., and Stupakov, G. V., "Flute Instability of Plasma in a Gas-Dynamic Trap," *Nuclear Fusion*, Vol. 24, No. 11, 1984, pp. 1421–1438.

[9]Coleman, H., and Steele, W., *Experimentation and Uncertainty Analysis for Engineers*, Wiley, New York, 1999, p. 49.

[10]Anderson, J. D., *Modern Compressible Flow: With Historical Perspective*, 2nd ed., McGraw–Hill, New York, 1990, p. 155.

[11]Kammash, T., *Fusion Reactor Physics*, Ann Arbor Science, Ann Arbor, MI, 1975, p. 333.

[12]Miyamoto, K., *Plasma Physics for Nuclear Fusion*, MIT Press, Cambridge, MA, 1980, p. 231.

[13]Ivanov, A. A., Anikeev, A. V., Bagryansky, P. A., Bocharov, V. N., Deichuli, P. P., Karpushov, A. N., Maximov, V. V., Podminogin, A. A., Rogozin, A. I., Salikova, T. V., and Tsidulko, Y. A., "Experimental Study of Curvature Driven Flute Instability in the Gasdynamic Trap," *Physics of Plasmas*, Vol. 1, No. 5, 1994, pp. 1529–1535.